mathematics

MDPI

Article

Hydrothermal Mixed Convection in a Split-Lid-Driven Triangular Cavity Suspended by NEPCM

Obai Younis [1], Sameh E. Ahmed [2,3,*], Aissa Abderrahmane [4], Abdulaziz Alenazi [5] and Ahmed M. Hassan [6]

[1] Department of Mechanical Engineering, College of Engineering in Wadi Addwasir, Prince Sattam Bin Abdulaziz University, Al-Kharj 11942, Saudi Arabia
[2] Department of Mathematics, Faculty of Science, King Khaild University, Abha 62529, Saudi Arabia
[3] Department of Mathematics, Faculty of Science, South Valley University, Qena 83523, Egypt
[4] Laboratoire de Physique Quantique de la Matière et Modélisation Mathématique (LPQ3M), University of Mascara, Mascara 29000, Algeria
[5] Department of Mathematics, College of Science, Northern Border University, Arar 73213, Saudi Arabia
[6] Department of Mechanical Engineering, Future University in Egypt, New Cairo 11835, Egypt
* Correspondence: sehassan@kku.edu.sa

Abstract: A numerical investigation of the magnetohydrodynamics of a mixed convection of nano-enhanced phase change material (NEPCM) within a triangular chamber containing an elliptical heat source is presented in this article. The forced convection has resulted from the movement of the upper cavity, while the free convection is due to the temperature difference between the heat source and cold inclined sidewalls. Four cases are considered based on the directions of the moving of the upper wall parts, namely, Case 1, where the left part is moving in the positive direction of the X-axis and the right part moves in the opposite direction ($1(+-)$), Case 2, where the two parts move in the positive direction of the X-axis ($2(++)$), Case 3, where the two parts move in the negative direction of the X-axis ($3(--)$), and Case 4, where the left part moves in the negative direction of the X-axis and the right part moves in the negative direction ($4(-+)$). The Galerkin finite element method (GFEM) is employed for addressing the governing equations of the system under study. The impacts of the Reynolds number ($1 \leq Re \leq 100$), the inclination angle of the elliptic heat source ($0 \leq \gamma \leq 90$), the nanoparticles volume fraction ϕ ($0\% \leq \phi \leq 8\%$) and the movement directions of the parts of the upper wall (four cases) are presented and discussed. The results suggested that increasing Re enhanced the heat transfer rate, while increasing Ha reduced it. The vertical positions of the elliptical heat source resulted in the maximum heat transmission rate. At the highest Re, changing the location of the heat source from horizontal ($\gamma = 0$) to vertical ($\gamma = 90$) enhanced the average Nusselt number by 60%, while choosing Case 1 for upper wall movement increased the average Nusselt number by 300% compared to Cases 2 and 3.

Keywords: mixed convection; GFEM; elliptic heat source; magnetic field; NEPCM

MSC: 76-10

Citation: Younis, O.; Ahmed, S.E.; Abderrahmane, A.; Alenazi, A.; Hassan, A.M. Hydrothermal Mixed Convection in a Split-Lid-Driven Triangular Cavity Suspended by NEPCM. *Mathematics* **2023**, *11*, 1323. https://doi.org/10.3390/math11061323

Academic Editors: Roman Parovik, Kholmat Mahkambaevich Shadimetov and Abdullo Rakhmonovich Hayotov

Received: 1 February 2023
Revised: 3 March 2023
Accepted: 6 March 2023
Published: 9 March 2023

1. Introduction

A practical method for containing the liquid phase of PCM and preventing its potentially hazardous interaction with the environment is the encapsulation of PCM (EPCM). Additionally, serving as a heat transfer surface, the encapsulating layer might sometimes also contribute to mechanical stability. Additionally, it enables the use of multiple PCMs in diverse applications [1–3]. In particular situations, such as when employing PCM for forced heat transfer by convection in a solid–liquid phase, it is difficult to use materials in the two-phase condition. The solution offered by encasing PCM in a shell is to get around both this and the limited heat conductivity of a PCM. Macro, micro and nanoscale techniques are used to create PCM capsules. PCMs contained in nanoscale capsules are called nano-encapsulated PCMs (NEPCMs). In the base liquid, such as water, NEPCMs are suspended. By heating the nanofluid to a certain temperature, NEPCMs can store vast quantities of thermal energy. The utilization of NEPCMs in energy storage systems is quite promising [4–6]. Ho et al. [7] evaluated the drop in pressure as well as the cooling efficiency of a mini channel heat sink loaded with NePCM. They discovered that, in a few specific cases, the cooling performance might be boosted up to 52%; however, in a few other cases, they reported that heat transmission deteriorated. Tahmasebi et al. [8] investigated the hydrodynamic and thermal characteristics of NEPCMs combined with the host fluid in glass balls as a permeable structure. The geometry is a 2D permeable square hollow in which the horizontal borders are believed to be insulated and the vertical boundaries produce the temperature differential. According to the findings, using a 5% concentration of NEPCMs might increase heat transmission by up to 20.1%. The concentration of NEPCMs is directly related to strengthening the heat transmission rate. The rate of heat transfer is also shown to be significantly affected by the non-dimensional fusion temperature. Li et al.'s [9] analysis of the nano-encapsulated PCM slurry soaked in metal foams resulted in the development of a novel, stable and effective model for passive thermal systems. They noted that this newly developed nano/foam-PCM combination not only produces greater heat transfer efficiency but also results in a reduction in the dependence on the convection coefficient. Seyf et al. [10] computationally studied the forced convection processes in octadecane NEPCMs (100 nm) with base liquid over an adiabatic cylinder. Assuming the motion to be stable and laminar, they conducted a parametric investigation on various nanoparticle concentrations. In another work [11], they provided a 3D model, measuring heat and fluid flow parameters affecting a micro-tube heat sink using NEPCMs as a coolant. They showed that nanoparticles had a positive effect on heat transmission, resulting in an increase in the cooling capacity of the investigated liquid; nevertheless, the presence of the particles caused a significant fall in pressure across the tube. A TES model was created by Alehosseini et al. [5] by taking into account the use of nano-micro encapsulated PCMs. Three kinds of nano-micro encapsulated PCMs were defined in this study using chemical, physio-mechanical and physio-chemical approaches. The natural convection of NEPCM inside a coaxial pipe has been researched by Ghalambaz et al. [12] According to their findings, 5% of NEPCM may increase the mean $\mathrm{Nu}_{\mathrm{Avg}}$ by around 73% when compared to water. In a different research work, Ghalambaz et al. [13] examined the results of adding NEPCMs to water in the presence of permeable material. They demonstrated that adding a 5% volume fraction of NEPCM may raise the average Nusselt number by 47%. Through a prismatic enclosure, Ahmed et al. [14] simulated fluid movement and heat transmission owing to radiation and convection. Nonadecane served as the NEPCM's core material in their investigation, while polyurethane served as the shell material. The simulation's findings demonstrate how substantially better heat transmission is achieved when using NEPCM. Hajjar et al. [15] investigated NEPCM unsteady free convection inside a chamber. One of their crucial results was an increase in mean Nu of up to 21% when the volume percentage of nanoparticles was increased from 2.5% to 5%. In an elliptical chamber with an inclined magnetic field, Seyyedi et al. [16] investigated the natural convection and entropy production of NEPCM. They observed that raising the Stefan number causes entropy to improve and the Nusselt number to decrease. In their study of the natural convection of NEPCMs within an enclosure, Ghalambaz et al. [17] found that the presence of NEPCM may result in the improvement of Nu. A few more relevant and helpful publications on the subject are addressed in Refs. [18–20].

Heat transmission and movement in a lid-driven chamber have received much interest from the research community. These investigations are regarded as a benchmark issue due to the ease with which the flow field may be explored or evaluated. A broad variety of engineering and natural processes, including fluid convection in the earth's core, waste disposal, crystal development, oceanography, the nuclear drying process, the cooling of electronic chips, solar collectors, etc., may use this issue. These applications are a few instances where a magnetic field's influence is crucial to regulating the fluid flow direction. As a result, the lid-driven chamber with a magnetic field has its own practical significance. Rostami et al. [21] investigated the movement and thermal distribution of a hybrid nanofluid flowing in a porous medium and over a stretched sheet under the influence of a magnetic field and dust particles. Significant study results indicate that raising the magnetic field parameter reduces the velocity profiles of nanofluid and dust particles by 16.86%, 16.8% and 15.41% for values of 0.1, 1, 2 and 3. Ahmed et al. [22] examined the mixed convection of Casson hybrid nanofluid within an inclined triangular container with a split-lid-driven wall and saturated with porous media. The container was also equipped with elliptic obstacles. The main results showed that the cold ellipse, $U_L = -1$ and $U_R = 1$ situations had the greatest rates of heat transmission. Additionally, the non-Newtonian hybrid nanofluid engine oil-Ti6Al4V + AA7075 improves the Nu_{Avg} more than the other variants. Hamzah et al. [23] examined the mixed convection and entropy formation in a permeability chamber triggered by a moving wavy lid and occupied by a CNT-water nanofluid in a magnetic field. Their findings showed that raising the Ri considerably increases the Nu number because of natural convection, and raising the Da number likewise raises the Nu number because of the influence of greater porosity on heat transmission. Ahmed et al. [24] looked into the effects of double lid-driven sidewalls, thermal radiation, heat absorption and the magnetic field on the convection heat transmission and nanofluid motion domain. The main findings showed that the convective process is enhanced by the expansion of the radiation and heat generation parameters. Additionally, as the magnetic parameter rises, the irreversibility of nanofluid friction takes precedence over that of heat transfer. A numerical simulation of a magneto-convection flow was performed by Laidoudi et al. [25] in a three-dimensional permeable chamber with a zigzag bottom wall and a sliding top wall. A hybrid nanofluid was placed within a permeable enclosure, and a magnetic field was applied. They discovered that accelerating the horizontal shift of the top wall or the permeability of the cavity boosts heat transmission and speeds up flow movement inside the enclosure. The movement of the flow particles is hampered by the application of the magnetic field, and the progressive increase in its strength has a detrimental effect on the heat transfer. The mixed convection of non-Newtonian nanofluids was studied by Zehba et al. [26] in a lid-driven tilted odd-shaped permeable chamber with obstructions. Under the combined impact of thermo-solubilization buoyant force and magnetic force in a moving lid chamber, Nath et al. [27] numerically examined the impact of nanoparticle form on heat and mass transport phenomena. The findings showed that the shape factor's impact on the Nusselt number depends significantly on the tilted magnetic field and buoyancy ratio; however, the shape influence on mass transfer is insignificant. In a hexagon-shaped container with a heated cylinder, Khan et al. [28] investigated the effects of a permeable material and an angled magnetic field on a natural convection nanofluid motion. According to their findings, the increasing porosity of the medium causes the heat transmission rates to exhibit a declining pattern at lower Darcy numbers. Mohammadpou et al. [29] presented an evolution of the LHTES study with the application of NEPCM through the statistical approach.

According to our knowledge, no prior research has looked into integrating NEPCM components with a lid-driven room with a triangular cross-section. Based on this, the analysis of the thermal transport inside a lid-driven chamber with moveable upper sides represents the core of this research. The inner obstacle is hot, while the lateral sides are cool. The development of refrigeration systems utilized in tiny electronic components can make use of this kind of result.

2. Problem Physics and Modeling

2.1. Physical Problem Description

In a two-dimensional triangular chamber with an elliptic heated wall and a moving split top-wall, the forced convection of a nanoliquid containing particles of an NEPCM is investigated. Figure 1 displays the enclosure's configuration.

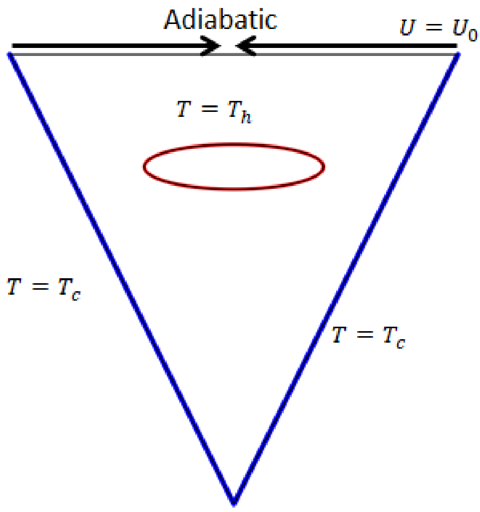

Figure 1. Physical problem and problem conditions.

The temperature of the hot wall is *Th*, while the temperature of the straight cold wall is kept constant at *Tc*. The higher and lower horizontal walls are called to be insulated. Furthermore, the gravitational field's parallel impacts on the temperatures of the cold and hot walls allow the buoyancy-driven flow to occur. Pressure changes have no effect on the density of nanoliquids. Temperature changes, in contrast, affect density. The particle distribution in the host fluid is uniform, and the nano-additives and base fluid have reached both dynamic and thermal equilibrium. Table 1 shows the thermophysical properties of the basic fluid as well as the chemicals utilized to make nanoadditives.

Table 1. Thermophysical properties of the NEPCMs and the base liquid [30–32].

Material	β (K^{-1})	C (kJ/kg K)	k (W/mK)	ρ (kg/m^3)
Polyurethane: shell	17.28×10^{-5}	1.3177		786
Nonadecane: core		2.037		721
Water: base fluid	21×10^{-5}	4.179	0.613	997.1

2.2. Assumptions and Equations

In response to the movement of a triangular cavity's split top wall, mixed convection flow develops. The water flow and the NEPCM are both two-dimensional, incompressible and constant. Consideration is also given to the Boussinesq approximation for fluctuations in linear density. The continuity, momentum and energy equations in $x - y$ directions are in this way [33]

$$\frac{\partial u}{\partial x} + \frac{\partial v}{\partial y} = 0 \tag{1}$$

$$\rho_m \left(u\frac{\partial u}{\partial x} + v\frac{\partial u}{\partial y} \right) = -\frac{\partial P}{\partial x} + \mu_m \left(\frac{\partial^2 u}{\partial x^2} + \frac{\partial^2 u}{\partial y^2} \right) - \frac{\mu_b}{K} u \tag{2}$$

$$\rho_m \left(u\frac{\partial v}{\partial x} + v\frac{\partial v}{\partial y} \right) = -\frac{\partial P}{\partial y} + \mu_m \left(\frac{\partial^2 v}{\partial x^2} + \frac{\partial^2 v}{\partial y^2} \right) - \sigma_m B_0^2 v - \frac{\mu_b}{K} v + (\rho\beta)_m (T - T_C) g \tag{3}$$

$$\left(u\frac{\partial}{\partial x}((\rho C_P)_m T) + v\frac{\partial}{\partial y}((\rho C_P)_m T) \right) = k_m \left(\frac{\partial^2 T}{\partial x^2} + \frac{\partial^2 T}{\partial y^2} \right). \tag{4}$$

u and v indicate the velocity elements in the x and y coordinates in the preceding statements. Moreover, P, T and g denote the pressure, temperature and acceleration of gravity in the y-direction, respectively. The source term for buoyant Boussinesq is the last term in Equation (3). In the energy conservation equation (Equation (4)), the advection term of NEPCMs influences. The functioning of NEPCM nanoparticles and their influence on problem performance will be explored in a subsequent section. Boundary conditions are required to complete the preceding linked formulae. Moreover, T_c is the temperature of the cavity's square walls and T_h is the temperature of the rotating cylinder. The velocity boundary conditions for the cold walls are nil, but the tangential velocity at the heated wall is r. We may eliminate dimensions from the governing equations by defining the following factors [34,35]:

$$\frac{\partial U}{\partial X}+\frac{\partial V}{\partial Y}=0 \tag{5}$$

$$\left(\frac{\rho_m}{\rho_{bf}}\right)\left(U\frac{\partial U}{\partial X}+V\frac{\partial U}{\partial Y}\right)=-\frac{\partial p}{\partial X}+\frac{1}{Re_{bf}}\left(\frac{\mu_m}{\mu_{bf}}\right)\left(\frac{\partial^2 U}{\partial X^2}+\frac{\partial^2 U}{\partial Y^2}-\frac{U}{Da}\right) \tag{6}$$

$$\left(\frac{\rho_m}{\rho_{bf}}\right)\left(U\frac{\partial V}{\partial X}+V\frac{\partial V}{\partial Y}\right)=-\frac{\partial p}{\partial Y}+\frac{1}{Re_{bf}}\left(\frac{\mu_m}{\mu_{bf}}\right)\left(\frac{\partial^2 V}{\partial X^2}+\frac{\partial^2 V}{\partial Y^2}-\frac{V}{Da}\right)+\frac{Gr_{bf}}{Re_{bf}^2}\left(\frac{(\rho\beta)_m}{(\rho\beta)_{bf}}\right)\theta-\frac{\sigma_m}{\sigma_{bf}}\frac{\mathrm{Ha}^2}{Re_{bf}}V \tag{7}$$

$$\left(U\frac{\partial}{\partial X}(Cr\theta)+V\frac{\partial}{\partial Y}(Cr\theta)\right)=\frac{1}{\mathrm{Re}_{bf}Pr_{bf}}\left(\frac{k_m}{k_{bf}}\right)\left(\frac{\partial^2\theta}{\partial X^2}+\frac{\partial^2\theta}{\partial Y^2}\right) \tag{8}$$

The dimensionless numbers are written as [33]:

$$v_{bf}=\frac{\mu_{bf}}{\rho_{bf}},\alpha_{bf}=\frac{k_{bf}}{\left(\rho c_p\right)_{bf}},\mathrm{Pr}=\frac{v_{bf}}{\alpha_{bf}},Re_{bf}=\frac{\omega r^2}{v_{bf}},Gr_{bf}=\frac{g\beta_{bf}\Delta Tr^3}{v_{\mathrm{bf}}{}^2}. \tag{9}$$

$v_{bf}, \alpha_{bf}, Pr, Re_{bf}$ and Gr_{bf} are the kinematic viscosity, thermal diffusion and Prandtl and Reynolds numbers, respectively [35]. Additionally, in Equations (5)–(9), (U, V) are the velocity components in the X- and Y-directions, respectively, θ is the dimensionless temperature and Da is the Darcy number. Additionally, the subscripts m and bf refer to the nanofluids and base fluid, respectively. In addition, the nondimensional number in the energy equation is the fraction of the heat capacity of the combination in relation to the heat capacity of the base liquid (Cr) [33].

$$Cr=\frac{(\rho C_P)_m}{(\rho C_P)_{bf}}=1-\varphi+\lambda\varphi+\frac{\varphi}{\chi}f \tag{10}$$

Parameters m and f in Equation (9) are the nanofluid combination and the base liquid, appropriately. The specific heat capacity and water density $(\rho C_\Gamma)_{bf}$ are unchanged. Nevertheless, given a certain base liquid and NEPCM material, the specific heat capacity values of the combination are dependent on the NEPCM volume percentage, the quantity of latent heat in the NEPCM core and the temperature (f). φ indicates variance with respect to volume percentage χ and illustrates the variance related with the NEPCM core's latent heat, and λ is determined using the formula [34]:

$$\lambda=\frac{(C_{p_{c,1}}+lC_{p_s})\rho_c\rho_s}{(\rho_s+l\rho_c)(\rho C_P)_{bf}} \tag{11}$$

λ is the fraction of the liquid phase heat capacity of NEPCM in relation to the base liquid, in which c, l and s represent the corresponding subscripts for core, liquid and sale. The l coefficient is equal to the fraction of the core in relation to the shell mass, which is 0.447. Additionally, in Equation (12), χ represents the ratio of a rise in the base fluid temperature to the latent heat stored in the core [33]:

$$\chi=\frac{C_{P,bf}}{h_{sf}/T_{Mr}}\frac{\rho_{bf}(\rho_s+l\rho_c)}{(\rho_s\rho_c)} \tag{12}$$

h_{sf} is the latent heat of the core, and T_{Mr} is the core's melting temperature range. In addition, the factor f in Equation (13) is the nondimensional fusion function derived from the following equation [34]:

$$f = \frac{\pi}{2}\sin\left(\frac{\pi}{\delta}\left(\theta - \theta_f + \frac{\delta}{2}\right)\right) \times \begin{cases} 0 \ if \ \theta < \theta_f - \frac{\delta}{2} \\ 1 \ if \ \theta_f - \frac{\delta}{2} < \theta < \theta_f + \frac{\delta}{2} \\ 0 \ if \ \theta < \theta_f + \frac{\delta}{2} \end{cases} \tag{13}$$

$$\delta = \frac{T_{Mr}}{\Delta T}, \text{ and } \theta_f = \frac{T_f - T_C}{\Delta T} \tag{14}$$

The terms θ_f, and δ denote the dimensionless temperature of fusion and internal fusion, respectively. As an alternative δ, it refers to the thickness of the melting zone. If the nanofluid temperature is greater than the NEPCM core melting temperature $\left(T > T_f + \frac{T_{Mt}}{2}\right)$ or lower than the core solidification temperature $\left(T > T_f + \frac{T_{Mt}}{2}\right)$, the final term of Equation (10) will be 0, and the values of Cr will decrease.

Cr is also affected by the melting temperature and melting range. Heat transmission can be enhanced by adjusting the Cr values. The greatest advantage of adopting NEPCMs over ordinary nanoparticles is the considerable increase in the specific heat capacity. The amplitude of the changing specific heat capacity in the two-phase condition is represented by the coefficient of the function f in Equation (13).

Additionally, the Cr values are smaller than one since NEPCM has a lower specific heat capacity than water, hence decreasing the specific heat capacity of the nanofluid. However, towards the phase transition zone, the specific heat capacity of the nanofluid rises significantly (identified in light blue). The Cr values given for $\chi = 0.01$.

The Nusselt number [36–43] may be used to determine the heat transmission rate.

$$Nu_{loc} = \frac{k_m}{k_{bf}}\frac{\partial\theta}{\partial n}, \ Nu_{\text{Ave}} = \frac{1}{\pi D}\int Nu_{loc}(n)dn. \tag{15}$$

where Nu_{loc} is the local Nusselt number, D is the diameter of the internal cylinder and Nu_{Avc} is the average Nusselt number.

2.3. Thermal-Physical Characteristics

A polyurethane shell surrounds a nonadecane core in nano-encapsulated PCM. The n-nonadecane is a suitable organic phase transition material for thermal energy storage, charging and solidifying at 31 °C, with a melting latent heat of 156.07 kJ/kg and a solidifying latent heat of 164.99 kJ/kg, respectively. As a result, this PCM may be used in buildings for thermal energy storage, and the operational temperature range as well as the quantity of energy that can be stored allow it to be used in buildings [44]. Researchers have evaluated the polyurethane shell because of its excellent elastic qualities, strength, smooth surface [45] and low crystallinity [15]. Furthermore, there are no environmental or health issues associated with formaldehyde leakage in this shell. In addition, the thermophysical characteristics of water and the specified NEPCM have been retrieved based on prior experimental findings [46]. Also discussed was the research on the synthesis of these nanoparticles for comparable uses [47]. The thermophysical characteristics of NEPCM may be presented by addressing both the core and shell thermophysical properties, as indicated [33]:

$$\rho_n = \frac{(1+l)\rho_c\rho_s}{\rho_s + l\rho_c} \tag{16}$$

where n denotes nanoparticle membership. As previously stated, the core's specific heat capacity may be written as a Sinusoidal function whose argument is a function of the temperature, fusion temperature $\left(T_f\right)$ and phase transition temperature range (T_{Mr}). The amplitude of this is also a function of the latent heat of the core $\left(h_{sf}\right)$, T_f and the specific heat capacity of the core in a liquid state $\left(C_{p_{c,l}}\right)$. Furthermore, the NEPCM core's specific heat capacity $\left(C_{p,c}\right)$ in the phase transition temperature range is [34]:

$$\begin{aligned} C_{p,c} = \quad & C_{p}c,t + \left\{\frac{\pi}{2}\left(\frac{h_{sf}}{T_{Mr}} - C_{pc,l}\right)\left(\sin\pi\frac{T-\left(T_f - T_{Mr}2\right)}{T_{Mr}}\right)\right\} \\ & \times\begin{cases} 0 \; if \; T < T_f - \frac{T_{Mr}}{2} \\ 1 \; if \; T_f - \frac{T_{Mr}}{2} < T < T_f + \frac{T_{Mr}}{2} \\ 0 \; if \; T < T_f + \frac{T_{Mr}}{2} \end{cases} \end{aligned} \tag{17}$$

The NEPCM's specific heat capacity and thermal expansion coefficient are as follows [33]:

$$\begin{aligned} C_{p,n} &= \frac{\left(C_{p,c} + lC_s\right)\rho_c\rho_s}{\left(\rho_s + l\rho_c\right)\rho_n} \\ \beta_n &= \beta_c + \left(\frac{\beta_s - \beta_c}{2}\right)\left(1 - \frac{l\rho_s}{\rho_c}\right) \end{aligned} \tag{18}$$

Considering the thermophysical characteristics of water, NEPCM nanoparticles and NEPCM volume portion, Table 1 presents the thermophysical parameters of the water–NEPCM combination. The following are thermophysical formulas for the mixture, including the density, specific heat capacity and thermal expansion coefficient [19,33]:

$$\begin{aligned} \rho_m &= (1-\varphi)\rho_{bf} + \varphi\rho_n \\ C_{P_m m} &= \frac{(1-\varphi)\rho_f C_{Pbf} + \varphi\rho_n C_{P,n}}{\rho_m} \end{aligned} \tag{19}$$

$$\beta_m = \frac{(1-\varphi)\rho_{bf}\beta_{bf} + \psi\rho_n\beta_n}{\rho_m} \tag{20}$$

The m, n and c indexes in all of the equations denote the mixture, NEPCM, core and shell, respectively. The current simulation was undertaken using a constant volume portion of 0.035. As a result, the dynamic viscosity and thermal conductivity of the mixture at 303 K are 0.7 $\mathrm{W/m \cdot K}$ and 122×10^{-5} $\mathrm{kg/m \cdot s}$, correspondingly, according to reference [46]. Table 1 also includes a list of the materials' thermophysical parameters.

2.4. The Computational Configuration, Mesh Independence and Validation

To evaluate if the equations were solved numerically, the Galerkin finite element method was used. Therefore, the equations have been quantitatively translated into the weak form. However, before the solution, the equations were changed into the weak form. Mesh study and independence are critical components of any numerical research. The domain was given with a structured sort of grid, as illustrated in Table 2. The average Nusselt number and maximum streamline value for these five situations are shown in Table 2, when *Re* = 100, *Ste* = 0.2, $\phi = 0$ and *N* = 4.

Table 2. Grid independence test for *Re* = 100, *Ste* = 0.2, $\phi = 0$ and *N* = 4.

No. of Elements	1632	2302	8987	23,362
$\Psi_{\max}$	−33.782	−33.736	−33.673	−33.673
Nu_a	7.8673	7.8078	7.8817	7.8815

In order to check the accuracy of the current results, the obtained outcomes are compared in special cases with those of Ghalambaz et al. [12]. This validation test is presented in Figure 2. It is noted that the features of the streamlines, isotherms and heat capacity ratio are in good agreement with those of Ghalambaz et al. [12].

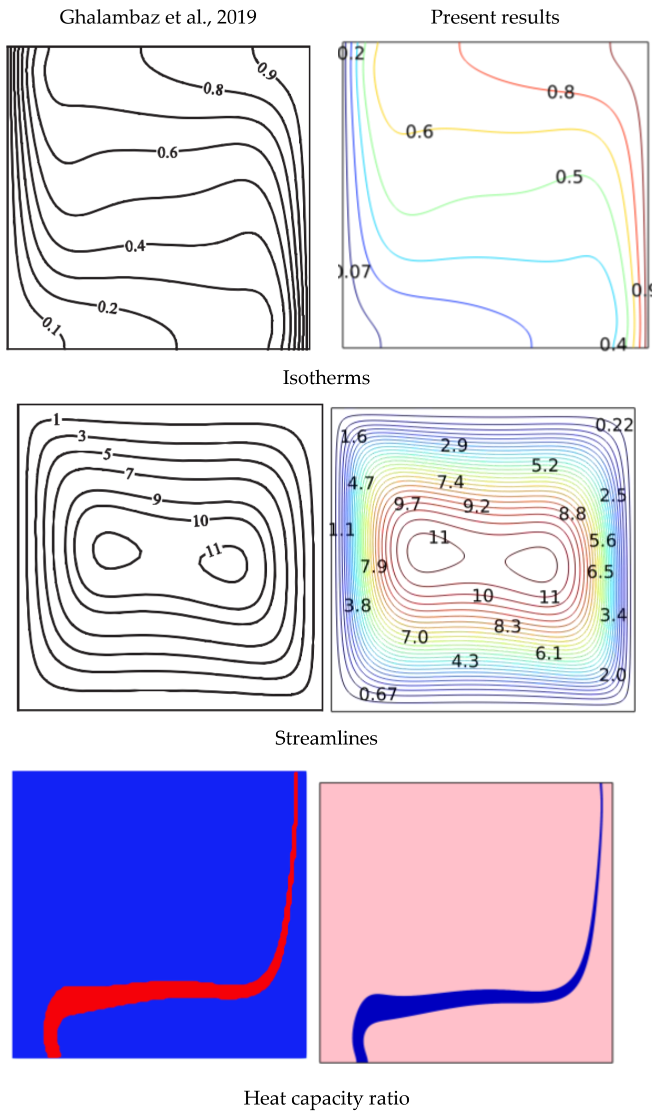

Figure 2. Comparison of isotherms, streamlines and heat capacity ratio with those of Ghalambaz et al. [12].

3. Results and Discussion

This part includes an overall discussion of the given outcomes. It is aimed, here, to explore the influences of the Reynolds number $(1 \leq Re \leq 100)$, the inclination angle of the elliptic shape γ $(0 \leq \gamma \leq 90)$ and the nanoparticles volume fraction ϕ $(0\% \leq \phi \leq 8\%)$. Additionally, various cases of the movement directions of the parts of the upper wall are considered, i.e., the right–left case $(1(+-))$, where the left part is moving in the positive direction and the right part is moving in the negative direction, the right–right case $(2(++))$, where the two parts of the upper wall are moving in the positive direction, the left–left case $(3(- -))$, where the two parts of the upper wall are moving in the negative direction, and the left–right case $(4(-+),)$ where the left part is moving in the negative direction and the right part is moving in a positive direction.

Figure 3 shows the features of the streamlines, temperature and capacity ratio of NECPCM Cr for the alteration of the Reynolds number Re. In this figure, the right–left case $(1(+-))$ is applied, and a vertically heated elliptic shape is included. It is noticeable that the opposite directions of the moving of the upper wall's parts cause the forming of two forced eddies near the upper edge. Additionally, the isotherms are distributed around the inner shape, indicating a dominance of the conduction mode compared to the convection situation at $Re = 1$. The growth in Re enhances the forced flow, and, hence, a strong flow is noted, with higher values of the stream function. Additionally, the temperature features show that the dominance of the convection case compared to the conduction mode is noted as *Re* increases. Additionally, an increase in the thickness of the thermal layers near the triangular edges is observed as *Re* is growing. In the same context, a ribbon feature around the inner shape is noted for the capacity ratio *Cr* at the lower values of *Re*, while, as *Re* is altered, the features of *Cr* are enhanced, indicating an enhancement in the melting–solidification process within the flow area.

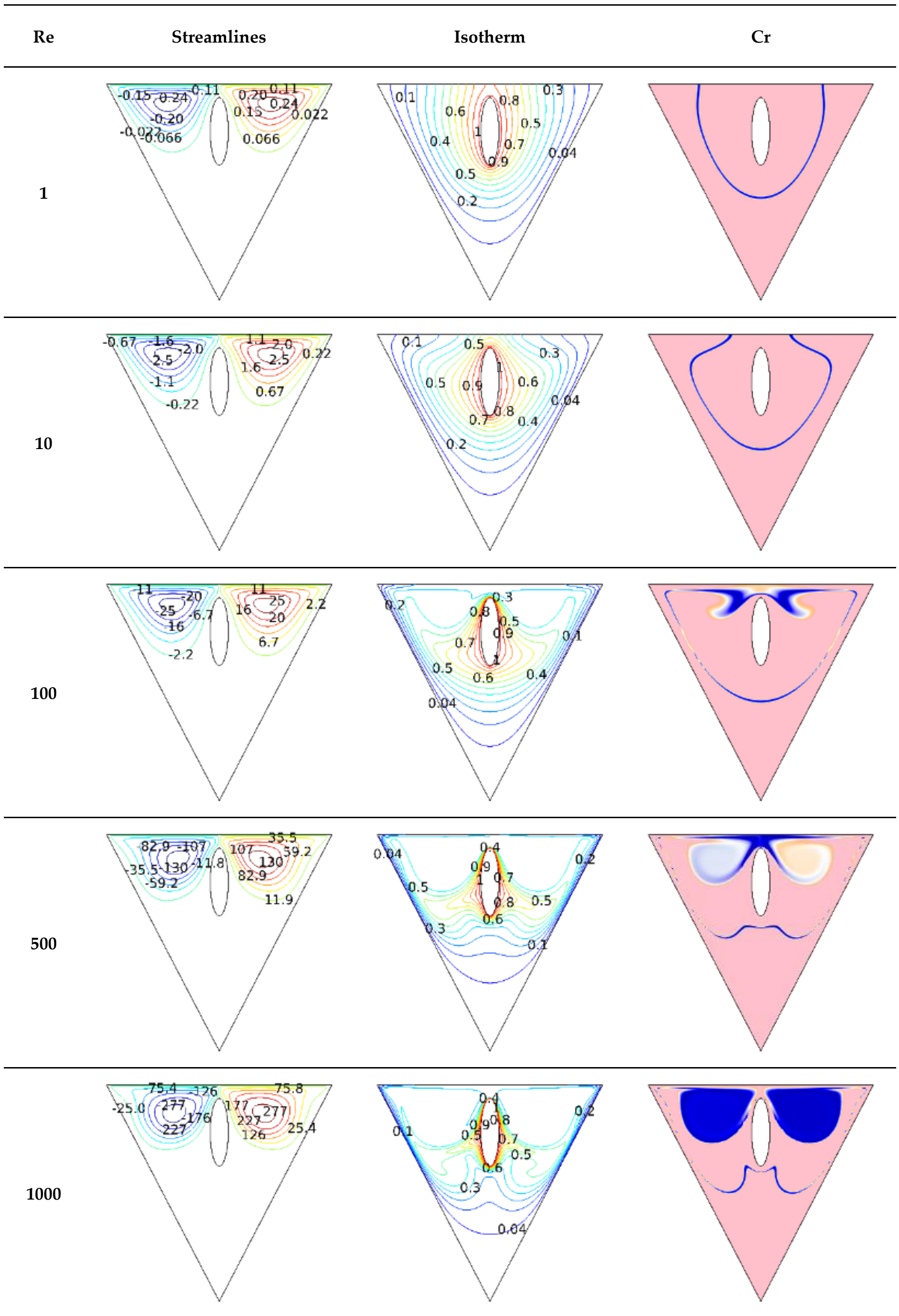

Figure 3. Features of the streamlines (**left**), isotherms (**middle**) and capacity ratio of NECPCM (**right**) for various values of Re. (The negative and positive sign numbers in the streamlines represent the direction and strength of flow, while the numbers in the isotherms mean the heating level).

In Figure 4, the inner-elliptic shape is inclined by various angles $\gamma = 0, 30, 60, 90$. The impacts of this rotation on the flow features, temperature and Cr distributions are examined using this illustration. Various configurations for the streamlines are seen as γ is varied. Here, the flow is symmetrical at $\gamma = 0$ and $\gamma = 90$, while an obstruction for the flow is seen in the right-hand side cell at $\gamma = 30$ and $\gamma = 60$. The isotherms revealed that the convection mode is enhanced in the horizontal and vertical cases, while the other values of γ cause a reduction in the isotherm gradients near the heated/cooled edges.

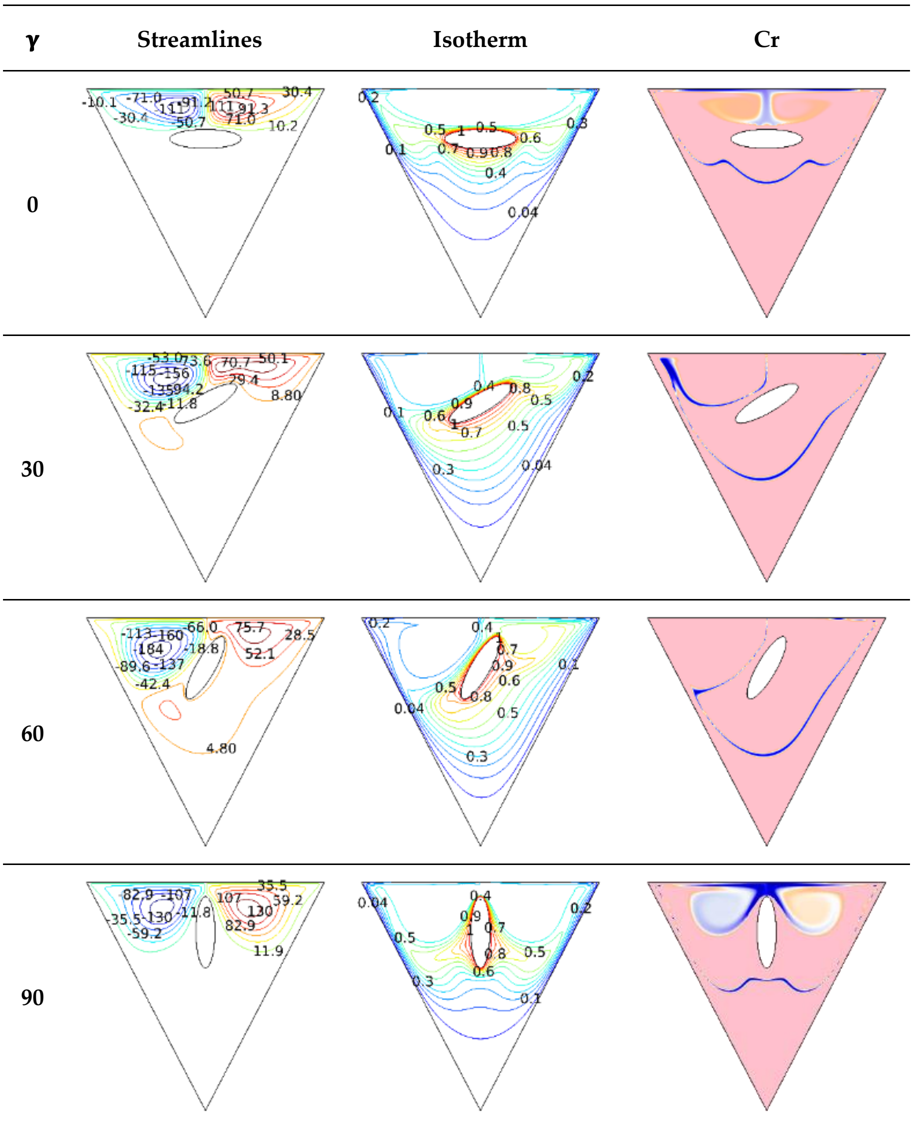

Figure 4. Features of the streamlines (**left**), isotherms (**middle**) and capacity ratio of NECPCM (**right**) for various values of γ. (The negative and positive sign numbers in the streamlines represent the direction and strength of flow, while the numbers in the isotherms mean the heating level).

Exploring the impacts of the movement direction of the upper wall parts on the flow structure, temperature distributions and ratio of the heat capacitance can be addressed using Figure 5. In this illustration, four cases are considered, namely, the right–left case (1(+−)), the right–right case (2(++)), the left–left case (3(− −)) and the left–right case (4(−+). It is noted that, in Case 1, the flow is represented by two clockwise and anti-clockwise vortices, and the distributions of the temperature have occurred in the middle area of the triangle. Additionally, the features of Cr are seen over the elliptic shape. In the same context, two opposite behaviors are noted for Case 2 and Case 3. In these cases, a major eddy is formulated, confined to the domain, and the melting–solidification process has occurred around the ellipsis. Case 4 causes the features of Case 1 to be reversed, and the temperature distributions are seen below the inner shape. All these features are due to the variations in the forced flow direction due to the movement of the upper parts.

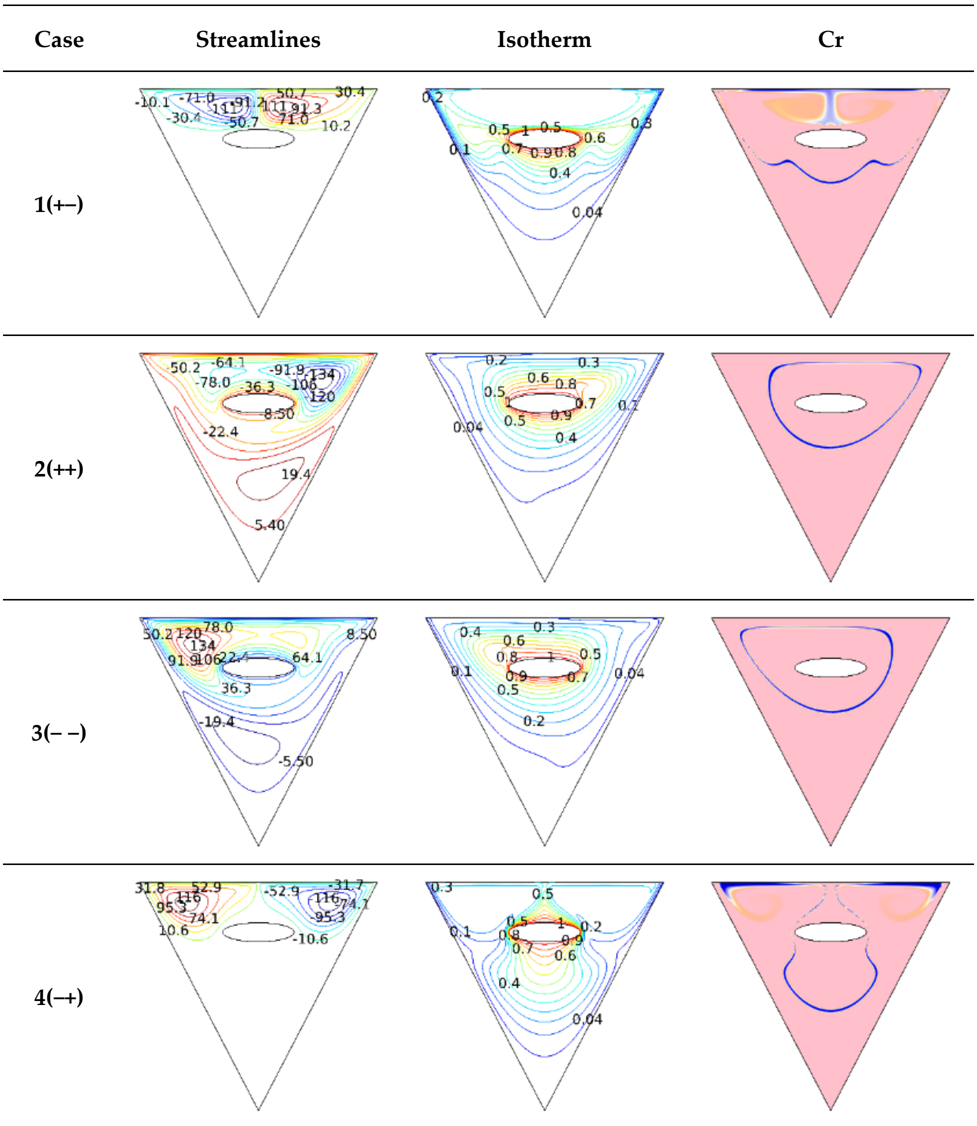

Figure 5. Features of the streamlines (**left**), isotherms (**middle**) and capacity ratio of NECPCM (**right**) for various considered cases. (The negative and positive sign numbers in the streamlines represent the direction and strength of flow, while the numbers in the isotherms mean the heating level).

Figure 6 displays the behaviors of the mean Nusselt issue Nu_{avg} and average Bejan number Be_{avg} for the alteration of ϕ and Re. The figure discloses that Nu_{avg} is enhanced significantly as Re is varied due to the enhancement in the temperature gradients, while the increase in ϕ leads to a small rise in the values of Nu_{avg} due to the rise in the suspension's thermal conductivity. Additionally, the values of Be_{avg} grow as Re is increased in the range of $Re > 1000$, while at $Re = 1000$, the values of Be_{avg} start to reduce. Physically, the alteration of Re causes the heat transfer irreversibility to be higher compared to the friction irreversibility; hence, Be_{avg} rises.

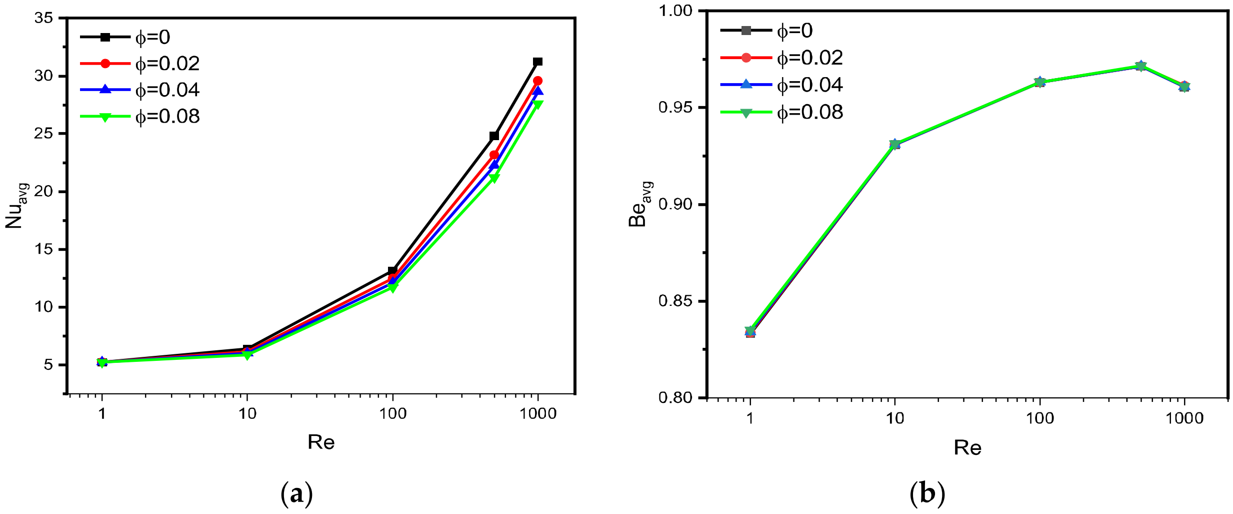

Figure 6. Effects of the nanoparticles volume fraction ϕ and Reynolds number Re on the (**a**) average Nusselt number $\mathrm{Nu}_{\mathrm{avg}}$ and (**b**) average Bejan number $\mathrm{Be}_{\mathrm{avg}}$ at Ha = 0, Ste = 0.2 and AR = 0.4.

Figure 7 depicts the behaviors of the mean Nusselt coefficient Nu_{avg} and mean Bejan issue Be_{avg} for the alteration of the elliptic-shaped inclination angle. It is noticeable that the vertically heated elliptical shape gives a higher rate of heat transfer, while $\gamma = 60$ gives lower values of Nu_{avg}. On the contrary, Be_{avg} obtains its higher values when the inner shape is inclined by $\pi/3$. It is also seen that the non-inclined shape causes that friction irreversibility to be dominant. In a related context, Figure 8 shows the significance of the movement direction of the upper parts on the mean values of the Nusselt and Bejan coefficients Nu_{avg} and Be_{avg}. Here, it should be mentioned that the opposite directions of the upper parts' movements give a higher heat transfer rate compared to the same direction. Additionally, the variations in Nu_{avg} against the considered cases are more noticeable on the higher values of Re compared to the lower values of Re. Furthermore, the features of Be_{avg} show that the heat transfer entropy in the right–right case (2(++)) and the left–left case (3($-$ $-$)) is significantly greater than the friction entropy.

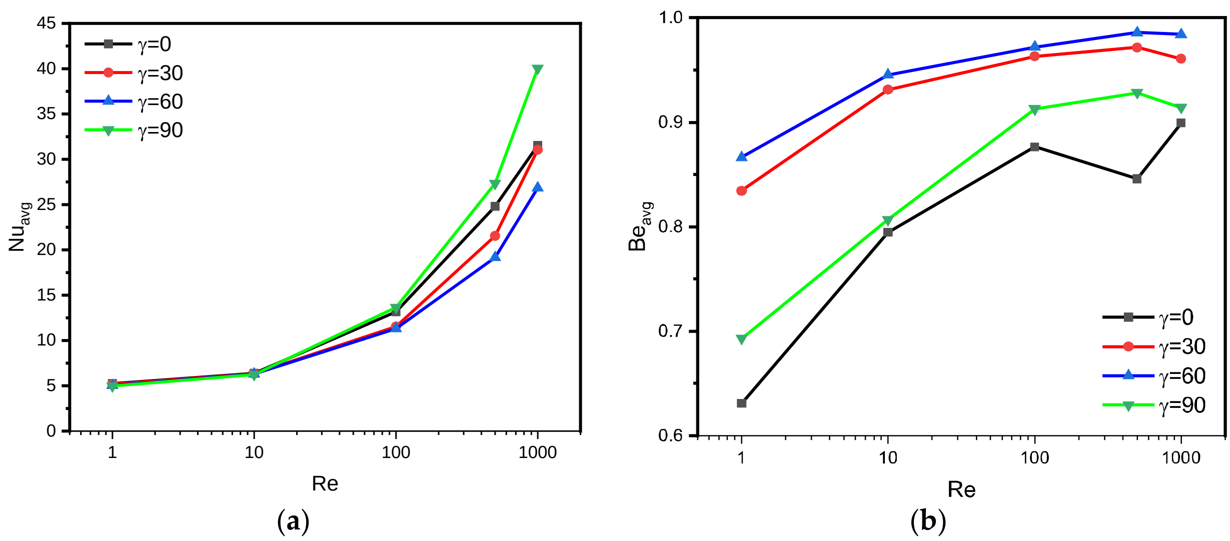

Figure 7. Effects of the elliptic-shaped inclination angle γ on the (**a**) average Nusselt number $\mathrm{Nu}_{\mathrm{avg}}$ and (**b**) average Bejan number $\mathrm{Be}_{\mathrm{avg}}$ at Ha = 0, and Ste = 0.2.

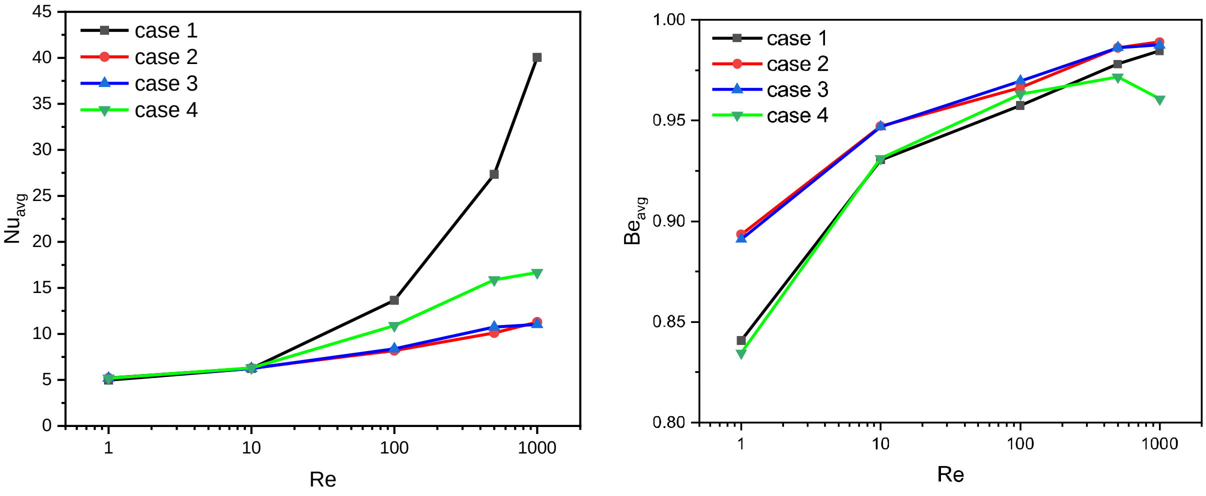

(**a**) (**b**)

Figure 8. Effects of the movement directions of the upper wall parts (Cases 1, 2, 3 and 4) on the (**a**) average Nusselt number Nu_{avg} and (**b**) average Bejan number Be_{avg} at Ha = 0 and *Ste* = 0.2.

Figure 9 displays the mean Nusselt coefficient Nu_{avg} for varied values of the Hartmann number Ha. Here, the range of Ha is considered between 0 and 100. The outcomes revealed that the growth in Ha causes a reduction in Nu_{avg} due to the Lorentz force, which works against the rate of heat transfer. In a related context, the local Nusselt number Nu_{loc} along the heated elliptic boundaries, according to the variations in Re, and the inner shape inclination angle are examined with the help of Figure 10. It is remarkable that Nu_{loc} is clearly enhanced as Re is altered due to the increase in the forced flow. Additionally, the vertical elliptic shape ($\gamma = 90$) gives higher values of Nu_{loc} compared to the other values of the angle. This behavior is because the heat distributions, in this case, are perpendicular to the direction of movement.

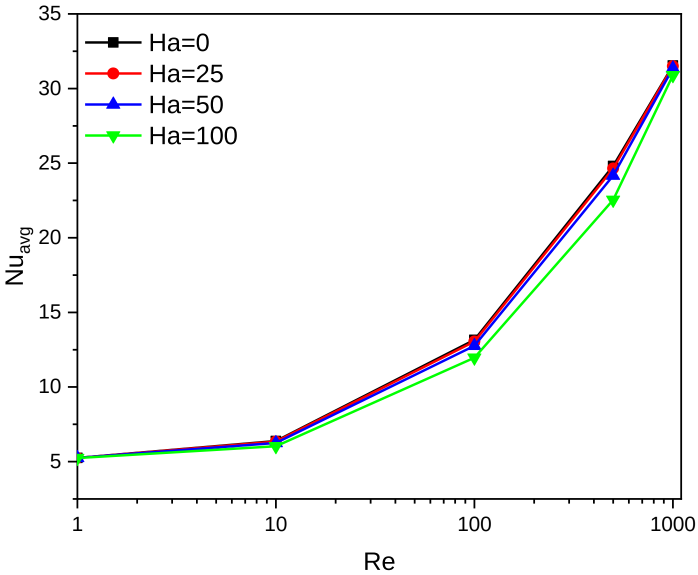

Figure 9. Effects of the Ha number on the Nu_{avg} at Ha = 0, *Ste* = 0.2.

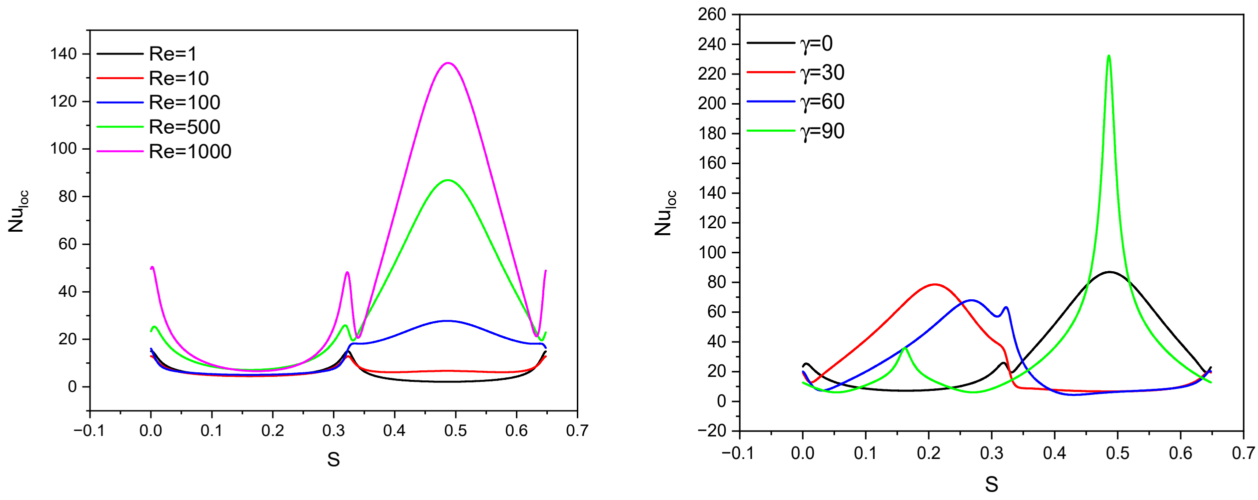

(**a**) (**b**)

Figure 10. Features of the local Nusselt number Nu_{loc} for (**a**) variations of the Reynolds number *Re* and (**b**) variations of the elliptic-shaped inclination angle γ at Ha = 0, *Ste* = 0.2.

4. Conclusions

Parametric simulations for the mixed convection situation due to the movements of a split-lid-driven wall of an acute triangular enclosure filled with NEPCM have been carried out. Four convective cases are considered based on the direction of the movement of the upper parts. These cases are the right–left case (1(+−)), the right–right case (2(++)) the left–left case (3(− −)) and the left–right case (4(−+). The flow domain was assumed to include an inclined inner elliptic shaper that has constant temperature distributions T_h. The magnetic field impacts were taken into account, and the solution methodology depends on the Finite Element Method. These simulations give the following major outcomes:

- The growth of *Re* enhanced the forced flow near the upper wall and, hence, the features of the flow; the isotherms and heat capacity ratio are supported.
- The vertical and horizontal elliptic shapes are better for maximizing the heat transfer rate.
- The opposite directions for the upper parts' movements enhance the flow and mean Nusselt coefficient.
- The horizontal heated ellipsis causes higher friction irreversibility compared to the other considered cases.
- The higher values of *Ha* reduce Nu_{avg}, regardless of the values of *Re*.
- The melting–solidification process is higher in the right–left case (1(+−)) compared to that in the other situations.
- In the future, three-dimensional melting cases and a variable magnetic field can be good generalizations of this study.

Author Contributions: Conceptualization, A.A. (Aissa Abderrahmane) and S.E.A.; funding acquisition, A.M.H.; methodology, A.A. (Aissa Abderrahmane) and O.Y.; writing—original draft, A.A. (Aissa Abderrahmane) and S.E.A.; writing—review and editing, A.A. (Abdulaziz Alenazi), O.Y. and S.E.A. All authors have read and agreed to the published version of the manuscript.

Funding: This research was funded by Deanship of Scientific Research at King Khalid University through the Large Groups Project under grant number (R.G.P2/64/44) and supported via funding from Prince sattam bin Abdulaziz University project number (PSAU/2023/R/1444).

Institutional Review Board Statement: Not applicable.

Informed Consent Statement: Not applicable.

Acknowledgments: The authors extend their appreciation to the Deanship of Scientific Research at King Khalid University for funding this work through the Large Groups Project under grant number (R.G.P2/64/44). This study is supported via funding from Prince sattam bin Abdulaziz University project number (PSAU/2023/R/1444).

Conflicts of Interest: The authors declare no conflict of interest.

Nomenclature

C	Mushy zone morphology constant
C_p	Heat capacity $(\mathrm{J/kg \cdot K})$
g	Gravity acceleration (m·s^{-2})
h_{ref}	Reference sensible enthalpy
K	Permeability of porous medium
k	Thermal conductivity $(\mathrm{W/m \cdot K})$
L	Latent heat coefficient $(\mathrm{KJ/kg})$
Pr_{bf}	Prandtl number
p	Pressure $(\mathrm{N/m^2})$
Re_{bf}	Reynolds number
Ste	Stefan number
T	Temperature (K)
T_s	PCM's solid temperature (K)
T_l	PCM's liquid temperature (K)
(u, v)	Velocity components $(\mathrm{m/s})$
Abbreviations	
NEPCM	Nano-Enhanced Phase Change Material
2D	Two-dimensional
LHTES	Latent heat thermal energy storage
HTF	Heat transfer fluid
$GFEM$	Galrkin Finite Element Method
Greek	
ρ	Density $(\mathrm{Kg/m^3})$
μ	Dynamic viscosity $(\mathrm{Pa \cdot s})$
α	Thermal diffusivity $(\mathrm{m^2/s})$
β	Thermal expansion coefficient $(1/\mathrm{K})$
φ	Volume fraction
Subscripts	
ref	Reference case
m	Nano-mixture
s	Solid
bf	Fluid

References

1. Tumirah, K.; Hussein, M.Z.; Zulkarnain, Z.; Rafeadah, R. Nano-encapsulated organic phase change material based on copolymer nanocomposites for thermal energy storage. *Energy* **2014**, *66*, 881–890. [CrossRef]
2. Ghoghaei, M.S.; Mahmoudian, A.; Mohammadi, O.; Shafii, M.; Mosleh, H.J.; Zandieh, M.; Ahmadi, M.H. A review on the applications of micro-/nano-encapsulated phase change material slurry in heat transfer and thermal storage systems. *J. Therm. Anal. Calorim.* **2021**, *145*, 245–268. [CrossRef]
3. Agresti, F.; Fedele, L.; Rossi, S.; Cabaleiro, D.; Bobbo, S.; Ischia, G.; Barison, S. Nano-encapsulated PCM emulsions prepared by a solvent-assisted method for solar applications. *Sol. Energy Mater. Sol. Cells* **2019**, *194*, 268–275. [CrossRef]
4. Sarı, A.; Alkan, C.; Döğüşcü, D.K.; Kızıl, Ç. Micro/nano encapsulated n -tetracosane and n -octadecane eutectic mixture with polystyrene shell for low-temperature latent heat thermal energy storage applications. *Sol. Energy* **2015**, *115*, 195–203. [CrossRef]
5. Alehosseini, E.; Jafari, S.M. Micro/nano-encapsulated phase change materials (PCMs) as emerging materials for the food industry. *Trends Food Sci. Technol.* **2019**, *91*, 116–128. [CrossRef]
6. Li, W.; Guo, S.; Tan, L.; Liu, L.; Ao, W. Heat transfer enhancement of nano-encapsulated phase change material (NEPCM) using metal foam for thermal energy storage. *Int. J. Heat Mass Transf.* **2020**, *166*, 120737. [CrossRef]
7. Ho, C.-J.; Chen, W.-C.; Yan, W.-M. Experimental study on cooling performance of minichannel heat sink using water-based MEPCM particles. *Int. Commun. Heat Mass Transf.* **2013**, *48*, 67–72. [CrossRef]

8. Tahmasebi, A.; Zargartalebi, H.; Mehryan, S.; Ghalambaz, M. Thermal and hydrodynamic behavior of suspensions comprising nano-encapsulated phase change materials in a porous enclosure. *Int. Commun. Heat Mass Transf.* **2020**, *116*, 104634. [CrossRef]
9. Li, W.; Zhang, D.; Jing, T.; Gao, M.; Liu, P.; He, G.; Qin, F. Nano-encapsulated phase change material slurry (Nano-PCMS) saturated in metal foam: A new stable and efficient strategy for passive thermal management. *Energy* **2018**, *165*, 743–751. [CrossRef]
10. Seyf, H.R.; Wilson, M.R.; Zhang, Y.; Ma, H.B. Flow and Heat Transfer of Nanoencapsulated Phase Change Material Slurry Past a Unconfined Square Cylinder. *J. Heat Transf.* **2014**, *136*, 051902. [CrossRef]
11. Seyf, H.R.; Zhou, Z.; Ma, H.; Zhang, Y. Three dimensional numerical study of heat-transfer enhancement by nano-encapsulated phase change material slurry in microtube heat sinks with tangential impingement. *Int. J. Heat Mass Transf.* **2013**, *56*, 561–573. [CrossRef]
12. Ghalambaz, M.; Chamkha, A.J.; Wen, D. Natural convective flow and heat transfer of Nano-Encapsulated Phase Change Materials (NEPCMs) in a cavity. *Int. J. Heat Mass Transf.* **2019**, *138*, 738–749. [CrossRef]
13. Ghalambaz, M.; Mehryan, S.; Mashoofi, N.; Hajjar, A.; Chamkha, A.J.; Sheremet, M.; Younis, O. Free convective melting-solidification heat transfer of nano-encapsulated phase change particles suspensions inside a coaxial pipe. *Adv. Powder Technol.* **2020**, *31*, 4470–4481. [CrossRef]
14. Ahmed, S.E.; Raizah, Z.A. Analysis of the entropy due to radiative flow of nano–encapsulated phase change materials within inclined porous prismatic enclosures: Finite element simulation. *J. Energy Storage* **2021**, *40*, 102719. [CrossRef]
15. Hajjar, A.; Mehryan, S.; Ghalambaz, M. Time periodic natural convection heat transfer in a nano-encapsulated phase-change suspension. *Int. J. Mech. Sci.* **2019**, *166*, 105243. [CrossRef]
16. Seyyedi, S.M.; Hashemi-Tilehnoee, M.; Sharifpur, M. Effect of Inclined Magnetic Field on the Entropy Generation in an Annulus Filled with NEPCM Suspension. *Math. Probl. Eng.* **2021**, *2021*, 8103300. [CrossRef]
17. Ghalambaz, M.; Zadeh, S.M.H.; Mehryan, S.; Haghparast, A.; Zargartalebi, H. Free convection of a suspension containing nano-encapsulated phase change material in a porous cavity; local thermal non-equilibrium model. *Heliyon* **2020**, *6*, e03823. [CrossRef]
18. Iachachene, F.; Haddad, Z.; Arıcı, M.; Abu-Nada, E.; Sheremet, M.A. The effect of nano encapsulated phase change materials and nanoparticles on turbulent heat transport: A conical diffuser scenario. *J. Energy Storage* **2022**, *52*, 104703. [CrossRef]
19. Abderrahmane, A.; Younis, O.; Al-Khaleel, M.; Laidoudi, H.; Akkurt, N.; Guedri, K.; Marzouki, R. 2D MHD Mixed Convection in a Zigzag Trapezoidal Thermal Energy Storage System Using NEPCM. *Nanomaterials* **2022**, *12*, 3270. [CrossRef]
20. Albdour, S.A.; Haddad, Z.; Sharaf, O.Z.; Alazzam, A.; Abu-Nada, E. Micro/nano-encapsulated phase-change materials (ePCMs) for solar photothermal absorption and storage: Fundamentals, recent advances, and future directions. *Prog. Energy Combust. Sci.* **2022**, *93*, 101037. [CrossRef]
21. Rostami, H.T.; Najafabadi, M.F.; Hosseinzadeh, K.; Ganji, D.D. Investigation of mixture-based dusty hybrid nanofluid flow in porous media affected by magnetic field using RBF method. *Int. J. Ambient. Energy* **2022**, *43*, 6425–6435. [CrossRef]
22. Ahmed, S.E.; Raizah, Z.A. Magnetic mixed convection of a Casson hybrid nanofluid due to split lid driven heat generated porous triangular containers with elliptic obstacles. *J. Magn. Magn. Mater.* **2022**, *559*, 169549. [CrossRef]
23. Hamzah, H.K.; Ali, F.H.; Hatami, M. MHD mixed convection and entropy generation of CNT-water nanofluid in a wavy lid-driven porous enclosure at different boundary conditions. *Sci. Rep.* **2022**, *12*, 2881. [CrossRef] [PubMed]
24. Ahmed, S.E.; Mahdy, A.; Mansour, M.A. Magnetic mixed convection confined two-sided wavy enclosures having two-sided lid-driven walls containing obstacles with thermal radiation. *Waves Random Complex Media* **2022**, 1–22. [CrossRef]
25. Laidoudi, H.; Abderrahmane, A.; Saeed, A.M.; Guedri, K.; Weera, W.; Younis, O.; Mourad, A.; Marzouki, R. Irreversibility Interpretation and MHD Mixed Convection of Hybrid Nanofluids in a 3D Heated Lid-Driven Chamber. *Nanomaterials* **2022**, *12*, 1747. [CrossRef]
26. Raizah, Z.; Aly, A.M.; Mansour, M.A. Radiative and heat generation effects on MHD mixed convection of non-Newtonian nanofluids in lid-driven inclined odd-shaped porous cavity containing obstacle using local thermal non-equilibrium condition. *Waves Random Complex Media* **2022**, 1–28. [CrossRef]
27. Nath, R.; Murugesan, K. Impact of nanoparticle shape on thermo-solutal buoyancy induced lid-driven-cavity with inclined magnetic-field. *Propuls. Power Res.* **2022**, *11*, 97–117. [CrossRef]
28. Khan, A.U.; Ullah, N.; Al-Zubaidi, A.; Nadeem, S. Finite element analysis for CuO/water nanofluid in a partially adiabatic enclosure: Inclined Lorentz forces and porous medium resistance. *Alex. Eng. J.* **2022**, *61*, 6477–6488. [CrossRef]
29. Mohammadpour, J.; Lee, A.; Timchenko, V.; Taylor, R. Nano-Enhanced Phase Change Materials for Thermal Energy Storage: A Bibliometric Analysis. *Energies* **2022**, *15*, 3426. [CrossRef]
30. Sadiq, M.A.; Alsabery, A.I.; Hashim, I. MHD Mixed Convection in a Lid-Driven Cavity with a Bottom Trapezoidal Body: Two-Phase Nanofluid Model. *Energies* **2018**, *11*, 2943. [CrossRef]
31. Maneengam, A.; Bouzennada, T.; Abderrahmane, A.; Guedri, K.; Weera, W.; Younis, O.; Bouallegue, B. Numerical Study of Lid-Driven Hybrid Nanofluid Flow in a Corrugated Porous Cavity in the Presence of Magnetic Field. *Nanomaterials* **2022**, *12*, 2390. [CrossRef]
32. Laidoudi, H.; Ameur, H. Complex fluid flow in annular space under the effects of mixed convection and rotating wall of the outer enclosure. *Heat Transfer* **2022**, *51*, 3741–3767. [CrossRef]

33. Ahmed, S.E.; Abderrahmane, A.; Alotaibi, S.; Younis, O.; Almasri, R.A.; Hussam, W.K. Enhanced Heat Transfer for NePCM-Melting-Based Thermal Energy of Finned Heat Pipe. *Nanomaterials* **2021**, *12*, 129. [CrossRef] [PubMed]
34. Ahmed, S.E.; Khamis, A.K. Exploration of the entropy due to the nano–encapsulated phase change materials (NEPCMs) within oblique prismatic containers. *Phys. Scr.* **2021**, *96*, 115204. [CrossRef]
35. Ahmed, S.; Abderrahmane, A.; Saeed, A.M.; Guedri, K.; Mourad, A.; Younis, O.; Botmart, T.; Shah, N.A. Melting enhancement of PCM in a finned tube latent heat thermal energy storage. *Sci. Rep.* **2022**, *12*, 11521. [CrossRef]
36. Liu, Y.; Upchurch, E.R.; Ozbayoglu, E.M. Experimental Study of Single Taylor Bubble Rising in Stagnant and Downward Flowing Non-Newtonian Fluids in Inclined Pipes. *Energies* **2021**, *14*, 578. [CrossRef]
37. Abu-Nada, E.; Chamkha, A.J. Mixed convection flow of a nanofluid in a lid-driven cavity with a wavy wall. *Int. Commun. Heat Mass Transf.* **2014**, *57*, 36–47. [CrossRef]
38. Wang, R.; Chen, T.; Qi, J.; Du, J.; Pan, G.; Huang, L. Investigation on the heat transfer enhancement by nanofluid under electric field considering electrophoretic and thermophoretic effect. *Case Stud. Therm. Eng.* **2021**, *28*, 101498. [CrossRef]
39. Hussain, S.; Jamal, M.; Geridonmez, B.P. Impact of fins and inclined magnetic field in double lid-driven cavity with Cu–water nanofluid. *Int. J. Therm. Sci.* **2020**, *161*, 106707. [CrossRef]
40. Du, J.; Wang, R.; Zhuo, Q.; Yuan, W. Heat transfer enhancement of Fe_3O_4 -water nanofluid by the thermo-magnetic convection and thermophorestic effect. *Int. J. Energy Res.* **2022**, *46*, 9521–9532. [CrossRef]
41. Narankhishig, Z.; Ham, J.; Lee, H.; Cho, H. Convective heat transfer characteristics of nanofluids including the magnetic effect on heat transfer enhancement—A review. *Appl. Therm. Eng.* **2021**, *193*, 116987. [CrossRef]
42. Selimefendigil, F.; Öztop, H.F. Natural convection and melting of NEPCM in a corrugated cavity under the effect of magnetic field. *J. Therm. Anal. Calorim.* **2019**, *140*, 1427–1442. [CrossRef]
43. Niazmand, A.; Sola, J.F.; Alinejad, F.; Dehgolan, F.R. Investigation of Mixed Convection in a Cylindrical Lid Driven Cavity Filled with Water-Cu Nanofluid. *Inventions* **2019**, *4*, 60. [CrossRef]
44. Jourabian, M.; Darzi, A.A.R.; Akbari, O.A.; Toghraie, D. The enthalpy-based lattice Boltzmann method (LBM) for simulation of NePCM melting in inclined elliptical annulus. *Phys. A Stat. Mech. Its Appl.* **2019**, *548*, 123887. [CrossRef]
45. Aly, A.M.; Mohamed, E.M.; El-Amin, M.F.; Alsedais, N. Double-diffusive convection between two different phases in a porous infinite-shaped enclosure suspended by nano encapsulated phase change materials. *Case Stud. Therm. Eng.* **2021**, *26*, 101016. [CrossRef]
46. Sadr, A.N.; Shekaramiz, M.; Zarinfar, M.; Esmaily, A.; Khoshtarash, H.; Toghraie, D. Simulation of mixed-convection of water and nano-encapsulated phase change material inside a square cavity with a rotating hot cylinder. *J. Energy Storage* **2021**, *47*, 103606. [CrossRef]
47. Abderrahmane, A.; Al-Khaleel, M.; Mourad, A.; Laidoudi, H.; Driss, Z.; Younis, O.; Guedri, K.; Marzouki, R. Natural Convection within Inversed T-Shaped Enclosure Filled by Nano-Enhanced Phase Change Material: Numerical Investigation. *Nanomaterials* **2022**, *12*, 2917. [CrossRef]